NUCL SCI TECH (2019) 30:143
https://doi.org/10.1007/s41365-019-0664-5

Ionizing and non-ionizing kerma factors in silicon for China Spallation Neutron Source neutron spectrum

Xiao-Ming Jin[1] · Yan Liu[1] · Chun-Lei Su[1] · Wei Chen[1] · Chen-hui Wang[1] · Shan-Chao Yang[1] · Xiao-Qiang Guo[1]

Received: 30 January 2019 / Revised: 2 April 2019 / Accepted: 5 May 2019 / Published online: 16 August 2019

Abstract The quantification of ionizing energy deposition and non-ionizing energy deposition plays a critical role in precision neutron dosimetry and in the separation of the displacement damage effects and ionizing effects induced by neutron radiation on semiconductor devices. In this report, neutrons generated by the newly built China Spallation Neutron Source (CSNS) are simulated by Geant4 in semiconductor material silicon to calculate the ionizing and non-ionizing kerma factors. Furthermore, the integral method is applied to calculate neutron-induced ionizing at the CSNS and non-ionizing kerma factors according to the standard neutron nuclear database and the incident neutron spectrum. In addition, thermoluminescence dosimeters are utilized to measure the ionizing energy deposition and six series of bipolar junction transistors are used to measure the non-ionizing energy deposition based on their neutron damage constants. The calibrated kerma factors that were experimentally measured agreed well with the simulation and integral calculation results. This report describes a complete set of methods and fundamental data for the analysis of neutron-induced radiation effects at the CSNS on silicon-based semiconductor devices.

Keywords Neutron radiation · Kerma · Ionizing energy · Non-ionizing energy · CSNS

1 Introduction

The kerma factor is defined as the sum of the initial kinetic energies of all the charged particles liberated by indirectly ionizing particles (for example, neutrons) in a volume element containing a unit mass of the specified material. The energy deposition per unit mass of the target material is the product of the fluence and the kerma factor. It is widely used in neutron radiation to quantitatively separate the ionizing energy deposition and non-ionizing energy deposition [1–5]. For semiconductor devices, neutron-induced radiation effects mainly include displacement damage, total ionizing dose (TID) effects, and single event effects (SEE). It has been proved that the displacement damage is equated with the non-ionizing kerma factor, so the 1 MeV equivalent neutron fluence has been commonly adopted for different neutron spectra for decades [6, 7]. Similarly, the TID and SEE are equated with the ionizing kerma factor of neutrons, which are directly related to the ionizing energy deposition induced by secondary ions owing to the interaction of incident neutrons with device materials [8–11].

The CSNS, located at Dongguan, Guangdong province in China, is the first spallation neutron source ever built in China and produces neutron spectra that are very similar to that of terrestrial neutrons. This scientific facility was initially opened to general users in 2018, and it has become one of the most significant neutron sources in China in terms of neutron radiation effects testing on semiconductor devices in avionics and spacecraft. Given that most

This work was supported by the National Natural Science Foundation of China (Nos. 11690040 and 11690043) and the Foundation of State Key Laboratory of China (Nos. SKLIPR1801Z and 6142802180304).

✉ Xiao-Ming Jin
jinxiaoming@nint.ac.cn

1 State Key Laboratory of Intense Pulsed Radiation Simulation and Effect, Northwest Institute of Nuclear Technology, No. 28, Pingyu Road, Baqiao District, Xi'an 710024, China

semiconductor devices are manufactured using silicon-based CMOS and bipolar technology, the ionizing and non-ionizing kerma factors in silicon are very important in the quantitative analysis of displacement damage and ionizing effects, respectively, as the fundamental data for neutron-induced radiation effects. Therefore, it is essential that the kerma factors should be confirmed for CSNS neutrons.

A comprehensive set of theoretical calculation methods and experimental calibration methods are proposed in this report to quantify the ionizing and non-ionizing kerma factors in silicon. Initially, ionizing and non-ionizing kerma factors are calculated using Geant4 simulation and the integral method, respectively. Moreover, thermoluminescence dosimeters are first calibrated using a standard Co-60 gamma irradiation source and are then irradiated in the CSNS neutron field to measure the ionizing dose and to calculate the experimental ionizing kerma factors. BJT transistors were first calibrated for their neutron damage constant in 1 MeV equivalent neutron fluence at Xi'an pulsed reactor (XAPR) [12] at the Northwest Institute of Nuclear Technology in China and were irradiated in the CSNS neutron field to calculate the experimental non-ionizing kerma factors via the normalization of the damage constant to 1 MeV neutron fluence.

2 Theoretical calculation

The CSNS is designed to deliver a proton beam with a kinetic energy of 1.6 GeV at a repetition rate of 25 Hz to a tungsten target [13, 14]. A tantalum (0.3 mm) clad and water-cooled sliced tungsten target (11 pieces, 65 cm in total length, cross section: 170 × 70 mm^2) are in use at the CSNS [15]. The investigations were performed at endstation 2# at a distance of 76 m from the tungsten target. Figure 1 shows the neutron energy spectrum at the sample

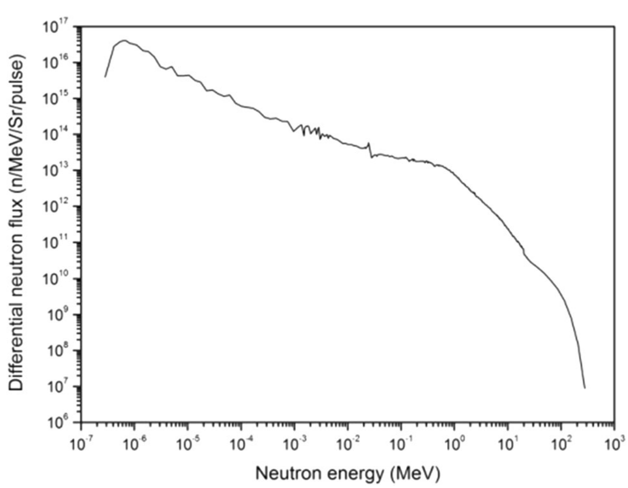

Fig. 1 Neutron energy spectrum at endstation 2# of the CSNS

position of endstation 2# of the CSNS. It was provided by CSNS staff using FLUKA 2011.2x software developed by European Organization for Nuclear Research. Approximately 14% of neutrons have energies from 0.28 eV to 0.1 MeV, 40% are from 0.1 to 1 MeV, 41% are from 1 to 20 MeV, and 5% are above 20 MeV. Two types of theoretical calculation methods including Geant4 simulation and the integral method were utilized to calculate the ionizing and non-ionizing kerma factors for the CSNS neutron beam based on the incident neutron spectrum.

2.1 Geant4 simulation

The geometrical structure established in Geant4 simulation consists of seven layers of silicon dielectric (Fig. 2). According to the feature size of current semiconductor technology, each layer is 100 μm in length and width and 20 μm in thickness. The direction of the incident neutrons is perpendicular to the surface of the first silicon layer, and the position of these neutrons is uniformly sampled in the x and y coordinates. The energy of the incident neutron is sampled from the initial neutron flux (Fig. 1). There are 252 continuous energy bins extending from 0.283 eV to 373.2 MeV. For each energy interval, the probability to initialize the energy of the incident neutron as the mean value of E_{i-1} and E_i is P_i, which is calculated using Eq. (1):

$$P_i = \frac{\int_{E_{i-1}}^{E_i} \Phi(E)\mathrm{d}E}{\int_{E_{\min}}^{E_{\max}} \Phi(E)\mathrm{d}E}, \tag{1}$$

where $\Phi(E)$ is the differential neutron flux for the CSNS neutrons, $E_{\min}$ is 0.283 eV, and $E_{\max}$ is 373.2 MeV.

A comprehensive set of physics lists are chosen to simulate the behavior of neutron transportation in silicon. Each physics list consists of a set of physics processes and cross sections for calculating total cross sections for a certain range of validity. The hadronic interactions were described by the QGSP_BIC_HP, the electromagnetic effects by the G4EmStandardNR, the decay process by the G4DecayPhysics, and the neutron interactions by the G4_NeutronHP. Moreover, the binary cascade model is implemented as an accurate intranuclear cascade model utilizing a realistic nucleon distribution model for the target nucleus, and the probability of collisions is based on the impact parameters between the incident particle and each of the target nucleons [16–18].

Ionization energy deposition is mainly due to electromagnetic processes due to secondary charged nucleons and nuclear fragments. Non-ionizing energy deposition is mainly attributed to the interaction of incident neutrons with target atoms and the Coulomb interaction of secondary charged nucleons with target atoms. Given that the

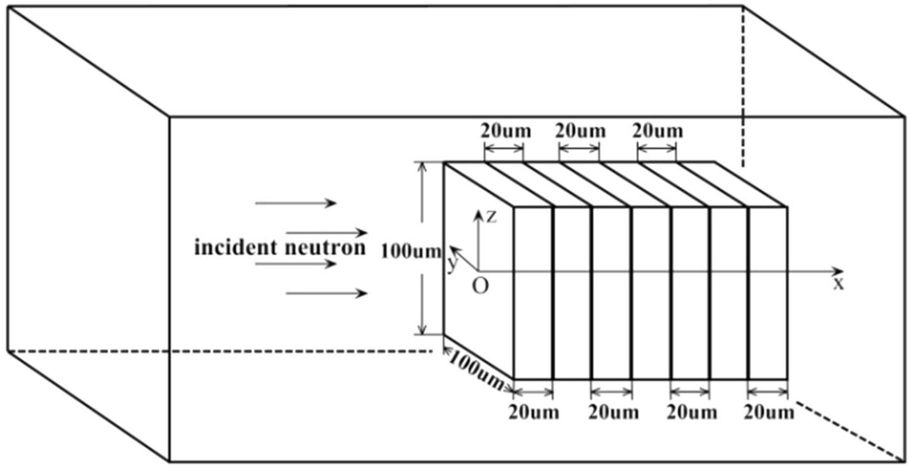

Fig. 2 Geometrical model for neutron transportation in silicon

thickness of silicon is much thinner than the range of incident neutrons in silicon, the energy deposition is uniformly distributed in each silicon layer and the cumulative ionizing and non-ionizing energy loss increases linearly with the thickness of silicon, as shown in Fig. 3. The ionizing and non-ionizing kerma factors can be calculated by the following equations:

$$K_{\mathrm{NIEL}} = \frac{1}{\rho}\frac{1}{N}\frac{\mathrm{d}E_{\mathrm{NIEL}}}{\mathrm{d}x}, \tag{2}$$

$$K_{\mathrm{IEL}} = \frac{1}{\rho}\frac{1}{N}\frac{\mathrm{d}E_{\mathrm{IEL}}}{\mathrm{d}x}, \tag{3}$$

where K_{NIEL} is the non-ionizing kerma factor, K_{IEL} is the ionizing kerma factor, N is the total sampling number for incident neutrons, and ρ is the density of silicon. In this work, $N = 10^7$, $\rho = 2.32$ g/cm^3, and $(\mathrm{d}E/\mathrm{d}x)/N$ is equal to the slope of the zero-crossing linear fitting. Finally, Geant4

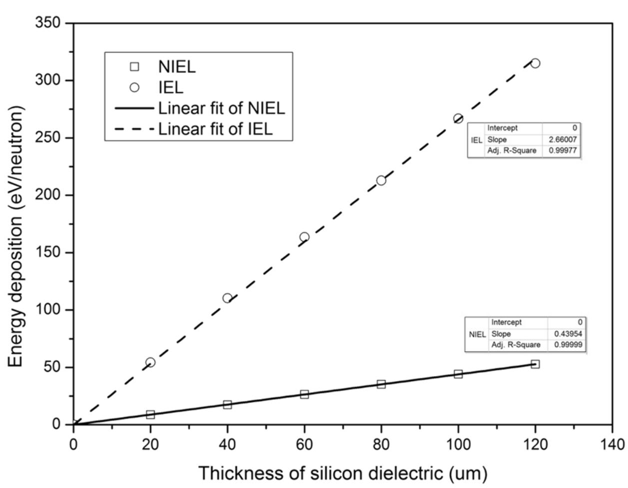

Fig. 3 Variation of the CSNS neutron-induced ionizing energy deposition and non-ionizing energy deposition as a function of the thickness of silicon

simulation results yield $K_{\mathrm{NIEL}} = 3.03 \times 10^{-13}$ Gy(Si) cm^2 and $K_{\mathrm{IEL}} = 1.83 \times 10^{-12}$ Gy(Si) cm^2.

2.2 Integral method

The kerma factor for CSNS neutrons via the integral method is calculated based on Eqs. (4) and (5) as follows:

$$K_{\mathrm{NIEL}} = \int_{E_{\min}}^{E_{\max}} \Phi(E) K_{\mathrm{NIEL}}(E)\mathrm{d}E, \tag{4}$$

$$K_{\mathrm{IEL}} = \int_{E_{\min}}^{E_{\max}} \Phi(E) K_{\mathrm{IEL}}(E)\mathrm{d}E, \tag{5}$$

where K_{NIEL} is the non-ionizing kerma factor for the CSNS neutrons, K_{IEL} is the ionizing kerma factor for the CSNS neutrons, E is the neutron energy, $\Phi(E)$ is the differential neutron flux for the CSNS neutrons, $K_{\mathrm{NIEL}}(E)$ is the non-ionizing kerma factor as a function of neutron energy E, $K_{\mathrm{IEL}}(E)$ is the ionizing kerma factor as a function of neutron energy E, $E_{\min}$ is the minimum energy of the CSNS neutrons, and $E_{\max}$ is the maximum neutron energy of the CSNS neutrons.

The kerma factors as a function of neutron energy are shown in Fig. 4. The non-ionizing kerma factors as a function of neutron energy are from the table of the silicon displacement function in ASTM E722-14 [4], and ionizing kerma function is obtained by subtracting the non-ionizing kerma function from the total kerma function for silicon, as indicated in Caswell's paper [5]. Finally, using the integral method, it was determined that $K_{\mathrm{NIEL}} = 2.96 \times 10^{-13}$ Gy(Si) cm^2 and $K_{\mathrm{IEL}} = 1.81 \times 10^{-12}$ Gy(Si) cm^2, exhibiting a good agreement with the Geant4 simulation results.

To further study the contribution of different neutron energy bands to the average kerma factor, the

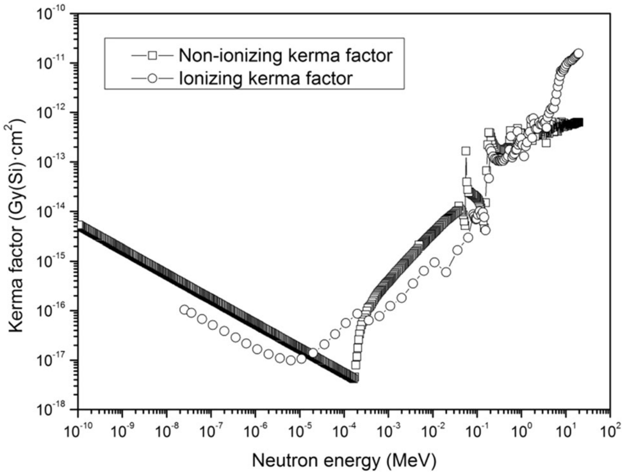

Fig. 4 Ionizing and non-ionizing kerma factors in silicon as a function of neutron energy

normalization of the integral of $K(E)\Phi(E)$ with respect to E as a function of neutron energy is shown in Fig. 5 for both non-ionizing and ionizing kerma functions. In the CSNS neutron spectrum, neutrons above 0.1 MeV account for 86% of the incident neutrons. These neutrons induce almost all the ionizing energy deposition and non-ionizing energy deposition in silicon.

3 Experimental verification

Experimental measurements were taken to validate the simulation and calculation results at the sample position of endstation 2# at a distance of 76 m from the tungsten target. To validate the ionizing kerma factor, thermoluminescence dosimetry was applied to obtain the ionizing dose under CSNS neutron irradiation. To validate the non-ionizing kerma factor, the neutron damage constants for a series of BJT transistors were measured in the CSNS neutron radiation environment.

3.1 Thermoluminescence dosimetry

Sensitive lithium fluoride-based thermoluminescence detectors (TLDs) doped with magnesium and titanium (^{7}LiF: Mg, Ti) was used to measure the absorbed radiation doses under CSNS neutron irradiation from fractions of μGy up to approximately the kGy range. The response of TLDs owing to neutron radiation is related to the neutron-induced ionizing dose deposition and the concomitant photon-induced ionizing dose deposition [19, 20]. The neutron-induced ionizing kerma factor could be calculated using the following equation:

$$\frac{\bar{R}}{s} = \frac{\frac{1}{m}\sum_{i=1}^{m} R_i}{s} = K_{\mathrm{IEL}}\Phi_{\mathrm{n}} + d_{\mathrm{p}}t_{\mathrm{r}} + B, \tag{6}$$

where R_i is the post-radiation readout value of the ith TLD by the thermoluminescence dosimeter reader, s is the TLD coefficient of the linear fitting slope of the average TLD calibration curve, m is the sample size of the TLDs (20 samples), K_{IEL} is the ionizing kerma factor for CSNS neutrons, Φ_{n} is the total irradiated neutron fluence of the TLDs [$(4.52 \pm 0.45) \times 10^{11}$ n/cm^2], d_{p} is the ionizing dose rate of the concomitant photons [$(2.62 \pm 0.02) \times 10^{-7}$ Gy(Si)/s measured by the CSNS staff], t_{r} is the total irradiated time of the TLDs [$(3.23 \pm 0.0001) \times 10^5$ s], and B is the ionizing dose of the natural background radiation [$(1.07 \pm 0.01) \times 10^{-3}$ Gy(Si) measured by additional TLDs].

The 20 TLD samples were calibrated at the Co-60 gamma radiation facility to determine the TLD coefficient, s. The calibration measurements were taken at multiple

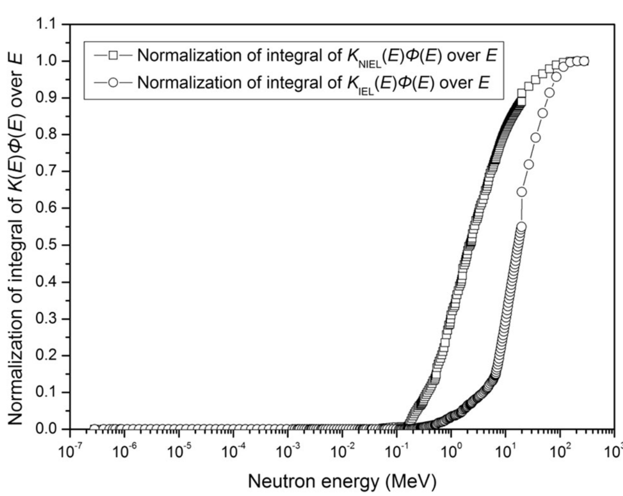

Fig. 5 Normalization of integral of $K(E)\Phi(E)$ with respect to E as a function of the neutron energy

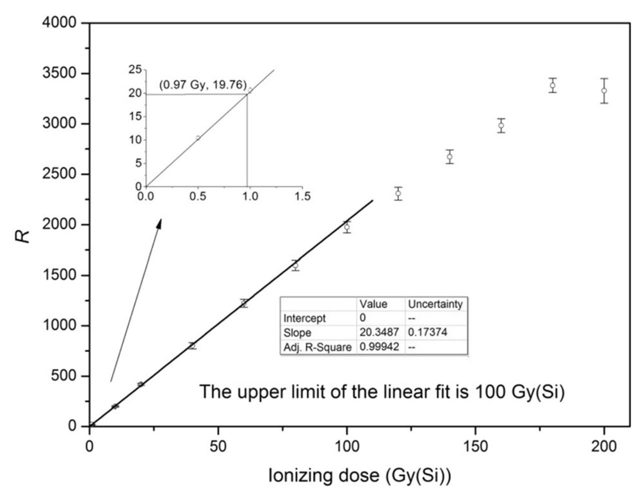

Fig. 6 The average readout value of the 20 TLDs versus ionizing dose for calibration measurements of TLD at Co-60

doses up to 200 ± 1 Gy(Si). Figure 6 represents the variation of the average readout value of the 20 TLD samples with the ionizing dose. This curve has good linearity between 0 and 100 ± 1 Gy(Si). Thus, its linearity upper limit is 100 ± 1 Gy(Si). The TLD coefficient s is the linear fitting slope of the average TLD calibration curve by Eq. (7):

$$\bar{R}(D) = \frac{1}{m}\sum_{i=1}^{m} R_i(D) = s \cdot D, \quad (7)$$

where D is the ionizing dose, $R_i(D)$ is the readout value of the ith TLD by the thermoluminescence dosimeter reader at ionizing dose D, and $\bar{R}(D)$ is the average readout value of the 20 samples at ionizing dose D. The TLD coefficient was determined to be 20.35 ± 0.17 Gy(Si)$^{-1}$ based on the linear fitting of measurements below 100 ± 1 Gy(Si).

In the CSNS experiment, the TLD samples were irradiated up to a total neutron fluence of (4.52 ± 0.45) × 10^{11} n/cm^2 at the sample position of endstation 2# for a distance of 76 m from the tungsten target, and the average readout value of the 20 TLDs $\bar{R}$ was 19.76 ± 0.12. Three additional TLD samples were placed in a natural radiation environment, accompanying the 20 TLD samples for neutron radiation testing during the entire experiment and transportation. The ionizing dose of the natural background radiation B was (1.07 ± 0.01) × 10^{-3} Gy(Si), as the average ionizing dose of the three TLDs. Therefore, based on thermoluminescence dosimetry, it was determined that the experimental K_{IEL} was (1.96 ± 0.20) × 10^{-12} Gy(Si) cm^2 using Eq. (6). This result is consistent with the theoretical calculation results.

3.2 Calibration of the BJT neutron damage constant

The radiation effects on BJTs and the displacement damage effects in silicon devices have been actively studied for almost six decades. One of the major achievements of the early studies on radiation effects was the development of the Messenger–Spratt equation, which demonstrates that the change in the current gain due to neutron irradiation is described as follows:

$$\Delta\frac{1}{\beta} = \frac{1}{\beta(\Phi)} - \frac{1}{\beta(0)} = k(\Phi), \quad (8)$$

where $\beta(0)$ is the pre-radiation current gain, $\beta(\varphi)$ is the post-radiation current gain, k is the neutron damage constant, and Φ is the neutron fluence [21]. In general, the mechanisms responsible for gain degradation in BJTs are attributable to displacement damage related to non-ionizing energy deposition [22]. Therefore, the constant k_{CSNS} for the CSNS and the k_{1MeV} for XAPR could be described as follows:

$$\frac{k_{\mathrm{CSNS}}}{k_{\mathrm{1MeV}}} = \frac{K_{\mathrm{NIEL}}(\mathrm{CSNS})}{K_{\mathrm{NIEL}}(\mathrm{1MeV})}, \quad (9)$$

where k_{CSNS} and k_{1MeV} are the constants that are determined from the linear fitting of the experimental results using Eq. (8) for the CSNS and XAPR, respectively. K_{NIEL}(CSNS) is the non-ionizing kerma factor for the CSNS neutron spectrum, K_{NIEL}(1 MeV) is equal to 3.27 × 10^{-13} Gy(Si) cm^2 (converted from 95 MeV mb in silicon according to ASTM E722-14 [4]).

The BJTs used for the radiation experiments were manufactured via a 0.8-um bipolar process by the State Key Laboratory of Analog Integrated Circuit, Chongqing, China. Table 1 summarizes the main features of six types of BJTs, including the transistor structure, emitter area, base region width, and base doping concentration.

During neutron irradiation, all the pins were shorted to ground. In the test interval after neutron exposure, the gain parameters of the transistors were measured using an HP4156A semiconductor parameter analyzer. For the PNP transistors, the collector was grounded, the emitter was biased to 2 V, and the base voltage was swept from 2 to 1 V. For the NPN transistors, the emitter was grounded, the collector was biased to 2 V, and the base voltage was swept from 0 to 1 V. The current gain β is the ratio of the collector current (fixed at 2 × 10^{-5} A for PNP and 6 × 10^{-4} A for NPN) and base current. Figure 7 shows the variation of 1/β with the neutron fluence at the CSNS and XAPR. The neutron fluence at the XAPR is 1 MeV equivalent neutron fluence. The experimental results illustrate a good linear relationship of $\triangle 1/\beta$ and the neutron fluence. The lateral PNP (PNP 1) is the most sensitive, the substrate PNPs (PNPs 2 and 3) are the second most sensitive, and the vertical NPNs (NPNs 1, 2, and 3) are the least sensitive in this study due to differences in the BJT structures. Linear fitting between $\triangle 1/\beta$ and the neutron fluence facilitates the calculation of the neutron damage constant k for each BJT for the CSNS and XAPR, respectively.

Figure 8 shows the neutron damage constants at the CSNS versus the XAPR for six types of BJTs. The slope of the linear fitting is 0.94 ± 0.03. Using Eq. (9), this slope indicates the ratio of the non-ionizing kerma factors between the CSNS and the XAPR. Therefore, the calibration method for the BJT neutron damage constant indicates that K_{NIEL} (CSNS) is (3.06 ± 0.10) × 10^{-13} Gy(Si) cm^2.

4 Discussion

As shown in Table 2, the non-ionizing and ionizing kerma factors for the CSNS neutrons are compared with the theoretical calculations and experimental validation. The difference is within 3.3% for non-ionizing kerma

Table 1 The bipolar transistors information

Description	Structure	Emitter area (μm^2)	Base region width (μm)	Base doping (cm^{-3})
PNP 1	Lateral	35 × 24	12	1.5×10^{15}
PNP 2	Substrate	66 × 28	11	1.5×10^{15}
PNP 3	Substrate	72 × 28	10	1.5×10^{15}
NPN 1	Vertical	250 × 20	11	8.0×10^{17}
NPN 2	Vertical	40 × 20	11	8.0×10^{17}
NPN 3	Vertical	50 × 50	5	8.0×10^{17}

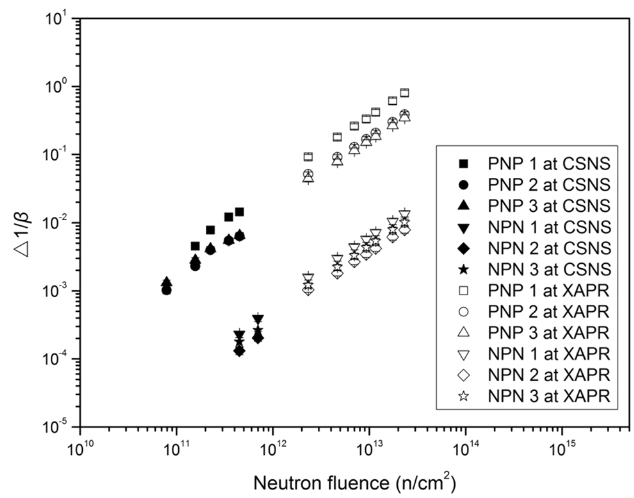

Fig. 7 Current gain degradation versus the increasing neutron fluence at the CSNS and the XAPR for the bipolar transistors

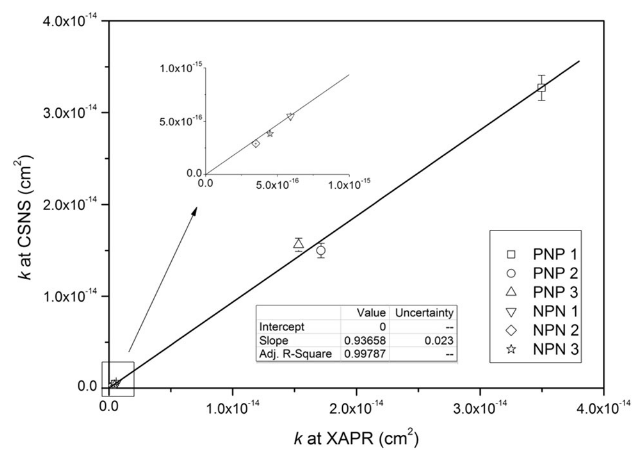

Fig. 8 Neutron damage constant k at the CSNS versus k at the XAPR for bipolar transistors. The slope of the linear fit represents the ratio of the non-ionizing kerma factors between the CSNS and the XAPR

factors and 6.7% for ionizing kerma factors. The neutron-induced displacement damage effects, especially for bipolar electronic devices, depend on the non-ionizing energy deposition, which is the product of the neutron fluence and non-ionizing kerma factor. Similarly, neutron-induced ionizing effects (for example, TID and SEE) depend on the ionizing energy deposition, which is the product of the neutron fluence and the ionizing kerma factor, especially for CMOS electronic devices. More importantly, the characterization of neutron radiation effects in electronic devices based on kerma factors facilitates uniformity of the interpretation and evaluation of the results of neutron irradiation via sources of different neutron energy spectra. As such, it is convenient to normalize the incident neutron fluence from a source to an equivalent monoenergetic neutron fluence (for example, 1 MeV equivalent neutron fluence) that is applicable to a particular semiconductor material (for example, silicon).

5 Conclusion

A comprehensive set of theoretical calculation methods and experimental calibration methods were presented to obtain and validate the neutron-induced non-ionizing and ionizing kerma factors in silicon. The experimental calibration results agree well with the theoretical results for the CSNS neutron spectrum. This consistency demonstrates that both the Geant4 simulation and the integral method for the standard database are appropriate approaches for the theoretical determination of the kerma factors. From an experimental perspective, the thermoluminescence dosimetry and the calibration method for the BJT neutron damage constant facilitate the determination of the ionizing and non-ionizing kerma factors, respectively. For the study

Table 2 Comparison of kerma factors between theoretical calculation and experimental validation for CSNS neutrons

Method	Non-ionizing kerma (Gy cm^2)	Ionization kerma (Gy cm^2)
Geant4 simulation	3.03×10^{-13}	1.83×10^{-12}
Integral method	2.96×10^{-13}	1.81×10^{-12}
Thermoluminescence dosimetry	–	$(1.96 \pm 0.20) \times 10^{-12}$
BJT neutron damage constant	$(3.06 \pm 0.10) \times 10^{-13}$	–

of radiation effects on semiconductor devices, the kerma factors allow us to separately quantify the non-ionizing energy deposition and ionizing energy deposition for a specified neutron fluence. The non-ionizing energy deposition is directly related to the displacement damage effects, especially for bipolar semiconductor devices, while the ionizing energy deposition is directly related to the TID and SEE effects, especially for CMOS semiconductor devices.

Acknowledgements The authors would like to express sincere appreciation to the collaborators for their contributions, particularly Jing-Yu Tang and Zhi-Xin Tan at CSNS and Guang-Ning Zhu and Qiang Zhang at XAPR.

References

1. V.P. Singh, N.M. Badiger, H.R. Vega-Carrillo, Neutron kerma factors and water equivalence of some tissue substitutes. Appl. Radiat. Isot. **103**, 115–119 (2015). https://doi.org/10.1016/j.apradiso.2015.05.014
2. Z.Z. Liu, J.X. Chen, New calculations of neutron kerma coefficients and dose equivalent. J. Radiol. Prot. **28**, 185–193 (2008). https://doi.org/10.1088/0952-4746/28/2/002
3. W.L. Bendel, Displacement and ionization fractions of fast neutron kerma in TLDs and Si. IEEE Trans. Nucl. Sci. **24**(6), 2516–2520 (1977). https://doi.org/10.1109/TNS.1977.4329248
4. Standard practice for characterizing neutron energy fluence spectra in terms of an equivalent monoenergetic neutron fluence for radiation-hardness testing of electronics. (Annual book of ASTM Standards E722-14, USA, 2007). https://doi.org/10.1520/e0722-14
5. R.S. Caswell, J.J. Coyne, M.L. Randolph, Kerma factors for neutron energies below 30 MeV. Radiat. Res. **83**(2), 217–254 (1980). https://doi.org/10.2307/3575276
6. J.R. Srour, J.W. Palko, Displacement damage effects in irradiated semiconductor devices. IEEE Trans. Nucl. Sci. **60**(3), 1740–1766 (2013). https://doi.org/10.1109/TNS.2013.2261316
7. J.R. Srour, C.J. Marshall, P.W. Marshall, Review of displacement damage effects in silicon devices. IEEE Trans. Nucl. Sci. **50**(3), 653–670 (2003). https://doi.org/10.1109/TNS.2003.813197
8. J.R. Schwank, M.R. Shaneyfelt, D.M. Fleetwood, J.A. Felix, P.E. Doddet, P. Paillet, V.F. Cavroisal, Radiation effects in MOS oxides. IEEE Trans. Nucl. Sci. **55**(4), 1833–1853 (2008). https://doi.org/10.1109/TNS.2008.2001040
9. T.R. Oldham, F.B. McLean, Total ionizing dose effects in MOS oxides and devices. IEEE Trans. Nucl. Sci. **50**(3), 483–499 (2003). https://doi.org/10.1109/TNS.2003.812927
10. D. Lambert, J. Baggio, V. Ferlet-Cavrois, O. Flament, F. Saigne, B. Sagnes, N. Buard, T. Carriere, Neutron-induced SEU in bulk SRAMs in terrestrial environment: simulations and experiments. IEEE Trans. Nucl. Sci. **51**(6), 3435–3441 (2004). https://doi.org/10.1109/TNS.2004.839133
11. F. Miller, C. Weulersse, T. Carriere, N. Guibbaud, S. Morand, R. Gaillard, Investigation of 14 MeV neutron capabilities for SEU hardness evaluation. IEEE Trans. Nucl. Sci. **60**(4), 2789–2796 (2013). https://doi.org/10.1109/TNS.2013.2241078
12. L.X. Chen, X.B. Tang, X.B. Jiang, D. Chen, Z.M. Zhao, Theoretical study on boiling heat transfer in the Xi'an pulsed reactor. Sci. China Technol. Sci. **56**(1), 137–142 (2013). https://doi.org/10.1007/s11431-012-5042-z
13. L.Y. Zhang, H.T. Jing, J.Y. Tang, X.Q. Wang, Design and simulations of the neutron dump for the back-streaming white neutron beam at CSNS. Radiat. Phys. Chem. **127**, 133–139 (2016). https://doi.org/10.1016/j.radphyschem.2016.06.023
14. J.B. Yu, J.X. Chen, L. Kang, J.F. Wu, J.Q. Zou, Thermal analysis and tests of W/Cu brazing for primary collimator scraper in CSNS/RCS. Nucl. Sci. Tech. **28**, 46 (2017). https://doi.org/10.1007/s41365-017-0208-9
15. L.Y. Zhang, H.T. Jing, J.Y. Tang, Q. Li, X.C. Ruan, J. Ren, C.J. Ning, Y.J. Yu, Z.X. Tan, P.C. Wang, Y.C. He, X.Q. Wang, Design of back-streaming white neutron beam line at CSNS. Appl. Radiat. Isot. **132**, 212–221 (2018). https://doi.org/10.1016/j.apradiso.2017.11.013
16. S. Agostinelli, Geant4—a simulation toolkit. Nucl. Instrum. Methods Phys. Res. Sect. A **506**, 50–303 (2003). https://doi.org/10.1016/s0168-9002(03)01368-8
17. S. Tripathi, C. Upadhyay, C.P. Nagaraj, K. Devan, A. Venkatesan, K. Madhusoodanan, Investigation of enhancement in planar fast neutron detector efficiency with stacked structure using Geant4. Nucl. Sci. Tech. **28**, 154 (2017). https://doi.org/10.1007/s41365-017-0315-7
18. P. Truscott, C. Dyer, A. Frydland et al., Neutron energy-deposition spectra measurements, and comparisons with Geant4 predictions. IEEE Trans. Nucl. Sci. **53**, 1883–1889 (2006). https://doi.org/10.1109/TNS.2006.880936
19. B. Obryk, R. Villari, P. Batistoni, A. Colangeli, P. De Felice, N. Fonnesu, M. Kłosowski, S. Loreti, K. Malik, J. Nash, M. Pillon, M. Pimpinella, L. Quintieri, J.E.T. Contributors, TLD calibration for neutron fluence measurements at JET fusion facility. Nucl. Instrum. Methods Phys. Res., Sect. A **904**, 202–213 (2018). https://doi.org/10.1016/j.nima.2018.07.050
20. J.R. Lei, Y.G. Yuan, L. Zhao, M.Z. Zhao, G.X. Gui, Investigations of the photon fluences in various $n + \gamma$ mixed fields in the fast neutron reactor. Acta Physica Sinica **52**(1), 53–57 (2003). https://doi.org/10.7498/aps.52.53
21. H.J. Barnaby, R.D. Schrimpf, K.F. Galloway, X. Li, J. Yang, C. Liu, Displacement damage in bipolar junction transistors: beyond Messenger–Spratt. IEEE Trans. Nucl. Sci. **64**(1), 149–155 (2017). https://doi.org/10.1109/TNS.2016.2615628
22. G.C. Messenger, M.S. Ash, *The Effects of Radiation on Electronic Systems* (Van Nostrand, New York, 1986). https://doi.org/10.1007/978-94-017-5355-5